This article has been accepted for publication in IEEE Antennas and Wireless Propagation Letters. This is the author's version which has not been fully edited and content may change prior to final publication. Citation information: DOI 10.1109/LAWP.2024.3368030

A Wideband Circularly Polarized Antenna with a Non-Uniform Metasurface Designed via Multi-Objective Bayesian Optimization

Yunjia Zeng, Xianming Qing, *Fellow, IEEE*, Michael Yan-Wah Chia

***Abstract*—A non-uniform metasurface circularly polarized patch antenna is designed using a genuine multi-objective Bayesian optimization (MOBO) method. Instead of aggregating the performance metrics into a single weighted sum, a genuine MOBO approach is adopted to explore the performance trade-offs, where three important antenna performance metrics, input impedance bandwidth, axial ratio (AR) bandwidth, and gain at boresight, are considered as the optimizing targets. Starting from a reference antenna with a uniform metasurface, the non-uniform metasurface antenna is designed by tuning ten physical design parameters automatically. The optimized antenna achieves an operating bandwidth of 25.6% (3.75 GHz–4.85 GHz) with $|S_{11}| < -10$dB, axial ratio less than 3 dB, and a maximum realized gain of 7.15 dBic. Compared with the reference antenna, the optimized design realizes a 31% enhancement in operating bandwidth while keeping the identical size of $1.12\lambda_0 \times 0.86\lambda_0 \times 0.069\lambda_0$ (λ_0 is the free space wavelength at center frequency of 4.3 GHz). Good agreement between measurement and simulation results validates the optimization methodology.**

***Index Terms*—Antenna, Microstrip Antenna, Metasurface, Circular Polarization, Multi-Objective Bayesian Optimization, 5G.**

I. Introduction

Circularly polarized (CP) antennas possess multiple distinct advantages as compared with the linearly polarized antennas, including reduced multipath interference, resilience to Faraday rotation effects of ionosphere, and mitigation of polarization mismatch loss. CP antennas have been applied in many wireless systems, including mobile communication [1], navigation, radar, Wi-Fi, and satellite systems. Among various types of CP antennas, single-fed microstrip CP antennas are indeed a popular solution for fulfilling the requirements of compact size, low profile, low fabrication cost, easy conformability, and simple configuration. However, single-fed microstrip CP antennas suffer from the inherent drawback of narrow bandwidths for both impedance and axial ratio (AR). Extensive research has been carried out to enhance the bandwidth of single-fed microstrip CP antennas, leading to the development of various approaches, including stacked patch structures with an air gap [2], capacitive probe feed with thick substrates [3], L-shaped strip feeding and shorting-pin loading [4], and meandering probe feed [5]. However, these approaches often necessitate the use of a thick substrate, which undermines the low-profile benefit of microstrip antennas.

Metasurfaces have been widely applied to improve the performance of different types of antennas [6]. One effective approach to improve the bandwidth of a single-fed microstrip CP antenna and maintain low profile is to apply a metasurface as a reactive impedance substrate [7]. The second method is to use a metasurface as a superstrate on top of the radiating patch in a single-fed microstrip CP antenna [8]. Another configuration is to utilize a metasurface as the radiating component and feed the metasurface via slot structure on the ground [9]. To further enhance the bandwidth of the CP antennas, a non-uniform metasurface was designed as the superstrate in [10]. A non-uniform metasurface with rectangular patches was proposed as the radiating structure in a single-fed CP antenna [11].

Among the global optimization methods, nature-inspired metaheuristic optimization methods such as genetic algorithms have long been applied in antenna design and optimization [12]. In recent years, there has been a growing application of Bayesian optimization (BO), another type of global optimization approach, in several studies focusing on the design and optimization of antennas [13-18]. Fundamentally different from the nature-inspired methods, BO is based on probabilistic modeling, utilizing a surrogate model to guide the search for the optimal solution by balancing exploration and exploitation of the search space. As a black-box global optimization approach, BO is particularly suitable to solve problems with complex physical models and expensive evaluation functions, which coincides with the cases of antenna designs with many design parameters.

Another important aspect of antenna design and optimization is that there are typically multiple conflicting objectives which may not be optimized at the same time without any compromise. To better facilitate the design trade-offs, genuine multi-objective (MO) optimization methods are essential to approximate the Pareto optimal set of such design problems. It has become a state-of-the-art technique in nature-inspired metaheuristic optimization methods, with many recent studies focusing on applying genuine MO approaches in antenna designs [19, 20]. Nonetheless, in the existing studies using BO for antenna designs, either single objective [13, 18]

Manuscript received 8 September 2023; revised 31 January 2024; accepted 17 February 2024. This work was partially supported by the Agency for Science, Technology and Research (A*STAR), Singapore, under its AME YIRG Fund (A2084c0173), National Research Foundation, Singapore and IMDA, under its Future Communication Programme.

Yunjia Zeng, Xianming Qing, Michael Yan-Wah Chia are with Institute for Infocomm Research, A*STAR, Singapore; e-mail: {zeng_yunjia; qingxm; michael_chia}@i2r.a-star.edu.sg.

This article has been accepted for publication in IEEE Antennas and Wireless Propagation Letters. This is the author's version which has not been fully edited and content may change prior to final publication. Citation information: DOI 10.1109/LAWP.2024.3368030

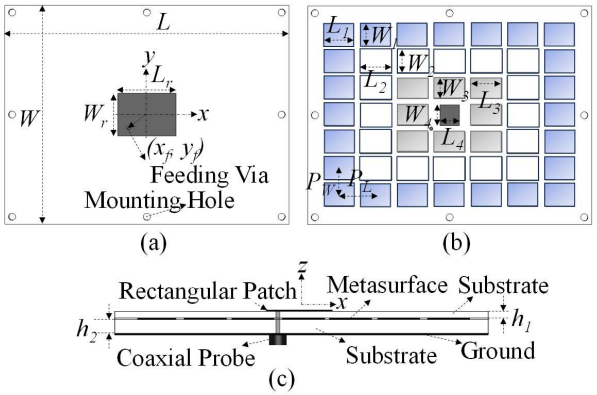

Fig. 1. Configurations of the non-uniform metasurface antenna: (a) top layer; (b) metasurface layer; (c) cross-sectional view.

was considered, or multiple objectives were aggregated into a single weighted sum [14-17], where the weighting coefficients are difficult to determine and can affect the optimization results significantly. In this sense, genuine multi-objective BO approaches are highly desirable to obtain the Pareto optimal set for antenna design and optimization. In this letter, a genuine multi-objective BO is applied to design and optimize a single-fed microstrip CP antenna with a non-uniform metasurface structure.

II. Non-Uniform Metasurface Patch Antenna and Objective Functions

The design in [21] is chosen as reference antenna, which consists of a rectangular patch radiator, a uniform 7 × 7 patch metasurface, and a ground. Fig. 1 shows the non-uniform metasurface antenna that is designed with the same configuration and size as the reference antenna for fair comparison. In both antennas, the rectangular patch radiator is positioned on the upper layer of the top substrate with a thickness of h_1. The metasurface is placed on the top layer of the lower substrate, which has a specified thickness of h_2. Both the substrates are made of FR4 with $\varepsilon_r = 4.2$, $\tan\delta = 0.022$. The patch radiator is excited via a coaxial probe at the feeding position of (x_f, y_f), through a feeding via with a diameter of 1 mm. The feeding position is fixed, and the size of the radiator is to be tuned, such that the relative feeding position on the radiator can be optimized. The drilled holes located near the edges of substrates are used for mounting and implementation purposes.

The introduction of non-periodicity greatly expands the design space. The 7 × 7 non-periodic metasurface structure includes a minimum of 98 design parameters, taking into account the length and width of each of the 49 patches. Even with the aid of Bayesian optimization, the computation cost involved is prohibitive. To overcome this challenge, the non-uniform metasurface is designed to be a concentric rectangular array with the same periodicities in *x*- and *y*- directions as the reference one. As shown in Fig. 1 (b), the patches along each concentric ring are of the same size and colored with the same

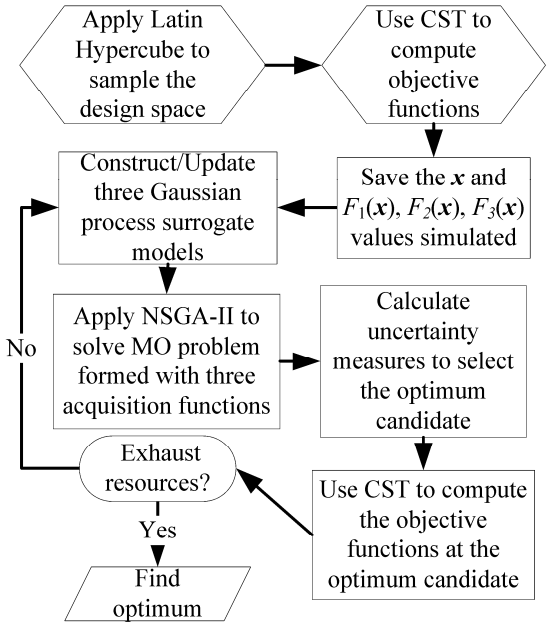

Fig. 2. Flowchart of the BO implementation.

shade. The corresponding sizes are (L_1, W_1), (L_2, W_2), (L_3, W_3), (L_4, W_4) from outermost rectangular ring to the innermost single patch, respectively.

The introduction of non-periodicity in the metasurface structure enables the excitation of multiple resonances, leading to a wide bandwidth. The non-uniform metasurface can be designed via altering the length L_i and width W_i along each concentric ring. Together with the size of the microstrip radiator (L_r, W_r), the vector of 10 design variables is expressed as $\boldsymbol{x} = [L_1, W_1, L_2, W_2, L_3, W_3, L_4, W_4, L_r, W_r]$. Note that the coordinates of the patch centers are fixed, and not considered as the design variables here, the inclusion of which will be a more general case to be studied in future.

The first objective in this case is to maximize the fractional bandwidth with reflection coefficient less than -10 dB within the desired frequency range of 3–5 GHz, which covers the operating bandwidth of the reference antenna. The second objective is to maximize the CP bandwidth with an axial ratio less than 3 dB in the targeted frequency range. In addition to the aforementioned considerations, another essential performance metric to be taken into account is the boresight realized gain across the frequency range. The design of the non-uniform metasurface antenna can be formulated as follows:

$$\begin{aligned} &\text{minimize } F_1(\boldsymbol{x}), F_2(\boldsymbol{x}), F_3(\boldsymbol{x}) \\ &\text{s.t. } \boldsymbol{x}^l \le \boldsymbol{x} \le \boldsymbol{x}^u, \end{aligned} \tag{1}$$

where

$$F_1(\boldsymbol{x}) = \frac{1}{m}\sum_{i=1}^{m} \max[S_{11}(\boldsymbol{x}, f_i) + 10, 0],$$
$$F_2(x) = \frac{1}{n}\sum_{i=1}^{n} \max[AR(x, fi) - 3, 0],$$
$$F_3(\boldsymbol{x}) = \frac{1}{p}\sum_{i=1}^{p} \max[10 - RG(\boldsymbol{x}, f_i), 0],$$

with $F_1(\boldsymbol{x})$, $F_2(\boldsymbol{x})$, and $F_3(\boldsymbol{x})$ as the three objective functions of real value, $\boldsymbol{x}^l$ and $\boldsymbol{x}^u$ represent the lower and upper bounds, respectively, of the design variables, *m*, *n*, and *p* are the number

TABLE I
GEOMETRIC DIMENSIONS OF THE OPTIMIZED ANTENNA (IN MM)

L	W	L_r	W_r	x_f	y_f	L_1	W_1	h_1
78.0	60.0	16.0	11.6	-5.1	-3.7	8.0	6.1	1.6
L_2	W_2	L_3	W_3	L_4	W_4	P_W	P_L	h_2
8.7	6.4	8.6	5.7	5.3	5.8	10.1	7.35	3.2

of sampling points in the desired frequency range for reflection coefficient, axial ratio and realized gain, respectively.

III. MULTI-OBJECTIVE BAYESIAN OPTIMIZATION AND DESIGN FLOW

Multi-objective (MO) Bayesian optimization with an uncertainty-aware search framework called UseMO [22] is employed to effectively address the design and optimization problem of non-uniform metasurface antenna described in Section II. The primary objective of USeMO is to identify the Pareto optimal set of solutions while simultaneously enhancing computational efficiency. A solution is considered Pareto optimal if it cannot be further enhanced in one objective without sacrificing another objective. The main idea of UseMO is to build multiple cheap suggorate statistical models of the real complex functions (in this case the computationally expensive electromagnetic simulations) for each of the objectives, and the corresponding acquisition functions can leverage on the existing ones in single-objective BO. The resulting MO problem is then solved using cheap MO solvers like NSGA-II [23], leading to a list of promising candidate sampling points. The candidate with maximum uncertainty is then identified via an uncertainty measure. The detailed formulations and theoretical analysis can be found in [22] and will not be covered here because of the scope of this work. The application of the UseMO on the design and optimization of the non-uniform metasurface antenna will be illustrated in detail below. Fig. 2 shows a chart of our design flow.

To begin with, the Latin Hypercube method is utilized to obtain 400 sampling points within the design space. The size of sampling data should be positively correlated with the number of design parameters as well as the number of design objectives. The number is determined based on the authors' experience and information from previous studies [13-18]. Each sample consists of 10 dimensions, namely, the vector $\boldsymbol{x}$ of 10 design variables as defined in Section II. The 10 variables vary in the ranges of: $2 \le L_1, L_2 \le 10.1, 2 \le W_1, W_2 \le 7.35, 2 \le L_3, L_4 \le 9, 2 \le W_3, W_4 \le 6, 8.82 \le W_r \le 20, 11.5 \le L_r \le 25$. The ranges are set in such a way that the patches in the outer two rings can overlap with each other, but the innermost patch and the third ring will not overlap with each other, such that the feeding via is not connecting to the patches on the metasurface. Each of the 400 design vectors, denoted as x, is simulated using CST [24] to determine the respective reflection coefficients, axial ratios, and realized gains to calculate the three objective functions $F_1(\boldsymbol{x})$, $F_2(\boldsymbol{x})$, and $F_3(\boldsymbol{x})$ as defined in (1). The 400 pairs of $\boldsymbol{x}$ and $F_1(\boldsymbol{x})$, $F_2(\boldsymbol{x})$, $F_3(\boldsymbol{x})$ obtained from the simulations of sample points are subsequently saved as the prior data and utilized to construct

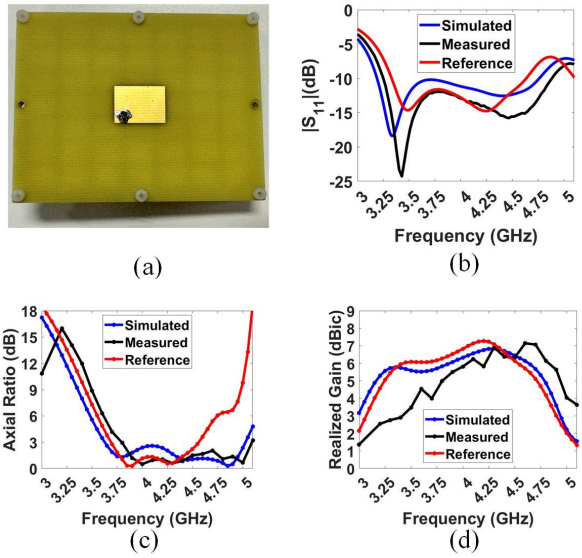

Fig. 3. Performance comparison with reference antenna [21]: (a) antenna prototype; (b) $|S_{11}|$; (c) axial ratio; and (d) boresight realized gain.

three probabilistic Gaussian process surrogate models $\widehat{F_1}(\boldsymbol{x})$, $\widehat{F_2}(\boldsymbol{x})$, and $\widehat{F_3}(\boldsymbol{x})$ with

$$\hat{F}(\boldsymbol{x}) \sim \mathrm{GP}(\mu(\boldsymbol{x}), k(\boldsymbol{x}, \boldsymbol{x'})), \tag{2}$$

where $\hat{F}(\boldsymbol{x})$ is the surrogate objective function, $\mu(\boldsymbol{x})$ and $k(\boldsymbol{x}, \boldsymbol{x'})$ are the mean and covariance functions. In this work, scaled absolute exponential kernel is chosen as the covariance function:

$$k(\boldsymbol{x}, \boldsymbol{x'}) = \mathrm{s}^2 \exp\left(-\frac{||x-x'||}{l}\right), \tag{3}$$

where s^2 and l are the scale and length-scale hyperparameters. The scikit-learn library in Python [25] is employed to fit the three Gaussian process models. The default values of the scale and length-scale hyperparameters are both set as 1, with the ranges of (10^{-3}, 10^3) and (10^{-6}, 10^6) as the bounds in hyper-parameter tuning, respectively.

When the iteration begins, three acquisition functions $\mathrm{AF}_1(\boldsymbol{x})$, $\mathrm{AF}_2(\boldsymbol{x})$, and $\mathrm{AF}_3(\boldsymbol{x})$ are constructed for each of the suggorate models, corresponding to each of the three objective functions in Section II. Common acquisition functions utilized in the optimization process include upper confidence bound (UCB), expected probability of improvement, and probability of improvement [22]. The UCB acquisition function used is in the form of

$$\mathrm{AF}(\boldsymbol{x}) = \mu(\boldsymbol{x}) + \beta_t^{1/2}\sigma(\boldsymbol{x}), \tag{4}$$

where $\mu(\boldsymbol{x})$ and $\sigma(\boldsymbol{x})$ are the mean and variance functions, β_t is the coefficient that finds the tradeoff between exploitation and exploration at iteration t. The adaptive β_t dependent on the iteration number is

$$\beta_t = \log(t^2\, 2\pi^2/0.3) + 0.125d\log(t^2) \tag{5}$$

where d is the dimension of input vector (10 in this case) [22]. NSGA-II is applied to solve the multi-objective optimization problem with the three acquisition functions as the objectives [22], [26].

This article has been accepted for publication in IEEE Antennas and Wireless Propagation Letters. This is the author's version which has not been fully edited and content may change prior to final publication. Citation information: DOI 10.1109/LAWP.2024.3368030

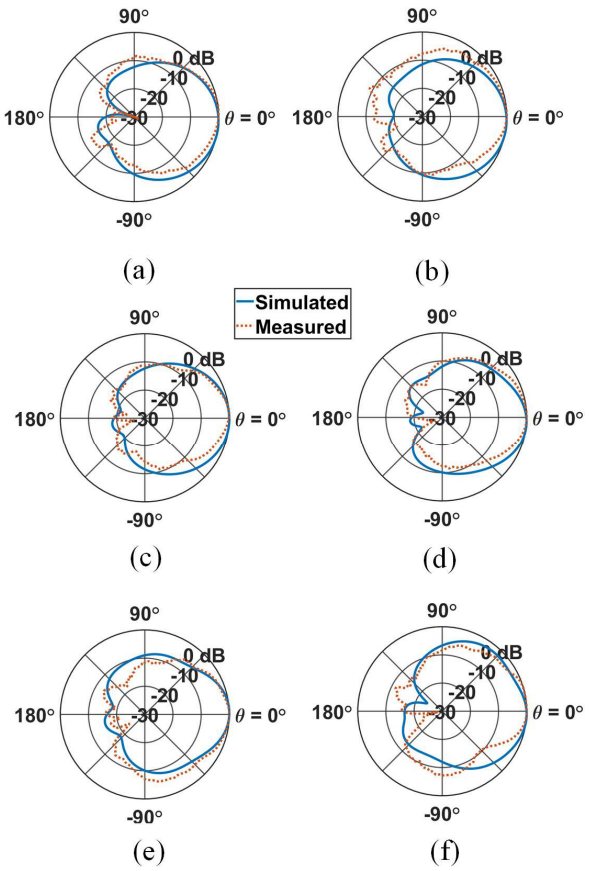

Fig. 4. Simulated and measured radiation patterns of the optimized antenna: (a) *xz*-plane and (b) *yz*-plane at 3.8 GHz; (c) *xz*-plane and (d) *yz*-plane at 4.3 GHz; (e) *xz*-plane and (f) *yz*-plane at 4.8 GHz.

Next, the uncertainty measures of the resulting list of candidate points obtained from NSGA-II are calculated as the volume of the confidence bounds of the statistical models [22]. The candidate point with the maximum uncertainty is then sent to CST for simulation with the results utilized to calculate the corresponding objective functions. The new pair of design variables $\boldsymbol{x}$ along with the corresponding objective values $F_1(\boldsymbol{x})$, $F_2(\boldsymbol{x})$, and $F_3(\boldsymbol{x})$ is then used to update the Gaussian process models. Furthermore, Like the previous applications [14, 17-18], the stopping criterion is set to be the predefined resource constraints. A predefined value of 1500 is assigned as the maximum number of iterations for the optimization process. Upon reaching the maximum number of iterations, all simulated results are collected, enabling the extraction of the optimal designs. The total computation time is 197.78 hours including the simulation time of the 400 prior data samples.

IV. Simulation and Measurement Results

The approximated Pareto optimal set of solution can be retrieved after the optimization completes. One optimal design is selected with the maximum operating bandwidth, which is the overlap between impedance and AR bandwidth, among all the designs that have a smaller-than 3dB variation in boresight gain across its bandwidth. The geometric dimensions of the optimized antenna are listed in Table I.

The antenna prototype as shown in Fig. 3(a) is measured in a full anechoic chamber. The measured results are compared with the simulated results. The reference in [21] is simulated as well for comparison. In Fig. 3(b), the optimized design achieves the measured impedance bandwidth of 3.25–4.85 GHz with $|S_{11}| < -10$dB, or fractional bandwidth of 39.5%. In [21], the reference antenna was measured with a VSWR ≤ 2 bandwidth of 34.2% (3.4 GHz–4.85 GHz). Fig. 3(c) shows that the measured 3-dB AR bandwidth of the optimized antenna ranges from 3.75 GHz to 5.05 GHz, achieving a fractional bandwidth of 29.5%, whereas the reference antenna in [21] only has a 3-dB AR bandwidth of 19.5% (3.7 GHz–4.5 GHz). Considering the overlap of impedance and AR bandwidth, the operating bandwidth of the optimized non-uniform metasurface antenna spans from 3.75 GHz to 4.85 GHz, or 25.6%, while the operating bandwidth of the reference design is 19.5% (3.7 GHz–4.5 GHz). Thus, the operating bandwidth of the optimized non-uniform design has a 31% enlargement as compared with that of the reference antenna.

Fig. 3(d) compares the simulated and measured realized gain of the prototype at boresight direction. The maximum realized gain of the optimized non-uniform antenna is 7.15 dBic, which is slightly less than that of the reference antenna (7.4 dBic) [21]. It is observed that the measured results are slightly shifted to higher frequency as compared with the simulated ones. The small discrepancies can be attributed to fabrication and assembly error.

To further examine the performance of the optimized antenna, Fig. 4 plots its radiation patterns at three frequencies, namely, the lower band edge, center frequency, and higher band edge across the operating bandwidth. The normalized measured and simulated radiation patterns are compared against each other in both *xz*- and *yz*- planes, with good agreement observed.

V. Conclusion

A wideband circularly polarized antenna with a non-uniform metasurface has been designed and optimized using a state-of-the-art genuine multi-objective Bayesian optimization approach. By properly exciting multiple resonances, the non-uniform antenna achieves a significant increment of 31% in operating bandwidth as compared with the periodic reference antenna, while still maintaining the low-profile feature as a single-fed microstrip antenna. As the non-uniformity prohibitively increases the design space, a concentric rectangular array configuration has been used in designing the metasurface to reduce the number of design variables. The genuine multi-objective Bayesian optimization approach is desired to explore the performance trade-offs and approximate the Pareto optimal set. The designed wideband circularly polarized antenna can be applied across various domains and applications, including satellite systems and sub-6GHz 5G New Radio.

REFERENCES

[1] A. Abdalrazik , A. Gomaa , and Ahmed A. Kishk, "A hexaband quad-circular-polarization slotted patch antenna for 5G, GPS, WLAN, LTE, and radio navigation applications", *IEEE Antennas Wireless Propag. Lett*., vol. 20, no. 8, pp. 1438 – 1442, Aug. 2021.

[2] K. Chung and A. Mohan, "A systematic design method to obtain broadband characteristics for singly-fed electromagnetically coupled patch antenna for circular polarization," *IEEE Trans. Antennas Propag*., vol. 51, no. 12, pp. 3239–3248, Dec. 2003.

[3] J. Kovitz and Y. Rahmat-Samii, "Using thick substrate and capacitive probe compensation to enhance the bandwidth of traditional CP patch antennas," *IEEE Trans. Antennas Propag*., vol. 62, no. 10, pp. 4970–4979, Oct. 2014.

[4] J. Wu, X. Ren, Z. Wang, and Y. Yin, "Broadband circularly polarized antenna with L-shaped strip feeding and shorting-pin loading," *IEEE Antennas Wireless Propag. Lett*., vol. 13, pp. 1733–1736, Sep. 2014.

[5] Q. Lin, H. Wong, X. Zhang, and H. Lai, "Printed meandering probe-fed circularly polarized patch antenna with wide bandwidth," *IEEE Antennas Wirel. Propag. Lett*., 13, pp. 654–657, Mar. 2014.

[6] J. Wang et al., "Metantenna: when metasurface meets antenna again," IEEE Trans. Antennas Propag, vol. 68, no. 3, pp. 1332–1347, Mar. 2020.

[7] L. Bernard, G. Chertier, and R. Sauleau, "Wideband circularly polarized patch antennas on reactive impedance substrates," *IEEE Antennas and Wireless Propag. Lett*., vol. 10, pp. 1015–1018, 2011.

[8] S. X. Ta and I. Park, "Low-profile broadband circularly polarized patch antenna using metasurface," *IEEE Trans. Antennas Propag*., vol. 63, no. 12, pp. 5929–5934, Dec. 2015.

[9] Y. Juan, W. Yang, and W. Che, "Miniaturized low-profile circularly polarized metasurface antenna using capacitive loading," *IEEE Trans. Antennas Propag*., vol. 67, no. 5, pp. 3527-3532, May 2019.

[10] T. T. Le, H. H. Tran, and A. A. Althuwayb, ''Wideband circularly polarized antenna based on a non-uniform metasurface,'' *Appl. Sci*., vol. 10, no. 23, p. 8652, Dec. 2020.

[11] F. A. Dicandia and S. Genovesi, "Characteristic modes analysis of non-uniform metasurface superstrate for nanosatellite antenna design," *IEEE Access*, vol. 8, pp. 176050–176061, 2020

[12] S. K. Goudos, P. D. Diamantoulakis, M. A. Matin, P. Sarigiannidis, S. Wan and G. K. Karagiannidis, "Design of Antennas through Artificial Intelligence: State of the Art and Challenges," *IEEE Communications Magazine*, vol. 60, no. 12, pp. 96-102, December 2022

[13] H. Li, J. Zhou, L. Kang, Z. Yang, and M. Wang, "Optimization design of skin antenna based on Bayesian optimization," in *Proc. Int. Symp. On Microwave, Antenna, Propag., and EMC Technologies (MAPE)*, Xi'an, China, Oct. 2017, pp. 78–83.

[14] A. Yang, W. Xue, C. Tian, J. Li, and L. Ye, "A Design of Silicon Based Horn Antenna Optimized Using Bayesian Optimization," *2020 IEEE 6th International Conference on Computer and Communications (ICCC)*, 2020, pp. 438-442.

[15] J. Zhou et al., "A trust-region parallel Bayesian optimization method for simulation-driven antenna design," *IEEE Trans. On Antennas and Propag*., vol. 69, no. 7, pp. 3966–3981, July 2021.

[16]] J. Li, A. Yang, C. Tian, L. Ye, and B. Chen, "Multi-fidelity Bayesian algorithm for antenna optimization," *Journal of Systems Engineering and Electronics*, vol. 33, no. 6, pp. 1119–1126, Dec. 2022

[17] Y. Zeng, X. Qing and M. Y. W. Chia, "Design of Wideband Mushroom Antennas Using Single- and Multi-Objective Bayesian Optimization," *2022 IEEE International Symposium on Antennas and Propagation and USNC-URSI Radio Science Meeting (AP-S/URSI),* Denver, CO, USA, 2022, pp. 485-486

[18] S. Yamamoto, K. Takegami and H. Kanaya, "Performance Optimization of a Slot Antenna using Bayesian Optimization," *2022 IEEE Radio and Wireless Symposium (RWS)*, Las Vegas, NV, USA, 2022, pp. 153-155

[19] S. Koziel and A. Pietrenko-Dabrowska, "Fast Multi-Objective Optimization of Antenna Structures by Means of Data-Driven Surrogates and Dimensionality Reduction," *IEEE Access*, vol. 8, pp. 183300-183311, 2020.

[20] Q.-Q. Li, Q.-X. Chu, Y.-L. Chang, and J. Dong, "Tri-objective compact log-periodic dipole array antenna design using MOEA/DGPSO," *IEEE Trans. Antennas Propag*., vol. 68, no. 4, pp. 2714–2723, Apr. 2020.

[21] Nasimuddin, X. Qing and Z. N. Chen, "Broadband circularly polarized antenna using metasurface," *2017 Progress in Electromagnetics Research Symposium – Fall (PIERS – FALL)*, pp. 2940–2944, Singapore, 2017,

[22] S. Belakaria, A. Deshwal, N. K. Jayakodi, J. R. Doppa, "Uncertainty-aware search framework for multi-objective Bayesian optimization," in *Proc. of the AAAI Conference on Artificial Intelligence*, April 2020, vol. 34, no. 06, pp. 10044–1005.

[23] K. Deb, A. Pratap, S. Agarwal and T. Meyarivan, "A fast and elitist multiobjective genetic algorithm: NSGA-II," *IEEE Trans. on Evolutionary Computation*, vol. 6, no. 2, pp. 182–197, April 2002.

[24] CST Studio Suite® [Online]. Available: https://www.3ds.com/products-services/simulia/products/cst-studio-suite/

[25] F. Pedregosa, et al. "Scikit-learn: machine learning in Python," *Journal of machine Learning research*, vol. 12, pp. 2825–2830, Nov. 2011.

[26] "Platypus - multiobjective optimization in Python — Platypus documentation." [Online]. Available: https://platypus.readthedocs.io/en/latest/